Macromolecules

Article

Cite This: Macromolecules 2018, 51, 4424−4434

pH-Responsive Saloplastics Based on Weak Polyelectrolytes: From Molecular Processes to Material Scale Properties

Gaulthier Rydzek,[*,†,‡] Amir Pakdel,[‡] Agnieszka Witecka,[§] Dayangku Noorfazidah Awang Shri,[∥] Fabien Gaudière,[⊥] Valeria Nicolosi,[‡] Parvaneh Mokarian-Tabari,[‡] Pierre Schaaf,[#] Fouzia Boulmedais,[⊥] and Katsuhiko Ariga[†,%]

[†]World Premier International Center for Materials Nanoarchitectonics (MANA), National Institute for Materials Science (NIMS), Tsukuba, Japan

[‡]Centre for Research on Adaptive Nanostructures and Nanodevices (CRANN) and Advanced Materials Bio-Engineering Research Centre (AMBER), School of Chemistry, Trinity College Dublin, Dublin, Ireland

[§]Institute of Fundamental Technological Research, Polish Academy of Sciences, Warsaw, Poland

[∥]Faculty of Mechanical Engineering, Universiti Malaysia Pahang, Pekan, Pahang, Malaysia

[⊥]CNRS, Institut Charles Sadron UPR 22, Université de Strasbourg, F-67000 Strasbourg, France

[#]UMR-S 1121, Biomatériaux et Bioingénierie, Institut National de la Santé et de la Recherche Médicale, 11 rue Humann, Cedex 67085 Strasbourg, France

[%]Graduate School of Frontier Sciences, The University of Tokyo, Kashiwa 277-0827, Japan

Supporting Information

ABSTRACT: Compact polyelectrolyte complexes (COPECs), also named saloplastics, represent a new class of material with high fracture strain and self-healing properties. Here, COPECs based on poly(methacrylic acid) (PMAA) and poly(allylamine hydrochloride) (PAH) were prepared by centrifugation at pH 7. The influence of postassembly pH changes was monitored chemically by ATR-FTIR, ICP, DSC, and TGA, morphologically by SEM, and mechanically by strain to break measurements. Postassembly pH stimuli misbalanced the charge ratio in COPECs, impacting their concentration in counterions, cross-link density, and polymer chain mobility. At the material level, changes were observed in the porosity, composition, water content, and mechanical properties of COPECs. The cross-link density was a prominent factor governing the saloplastic's composition and water content. However, the porosity and mechanical properties were driven by several factors including salt-induced plasticization and conformational changes of polyelectrolytes. This work illustrates how multiple-scale consequences arise from a single change in the environment of COPECs, providing insights for future design of stimuli-responsive materials.

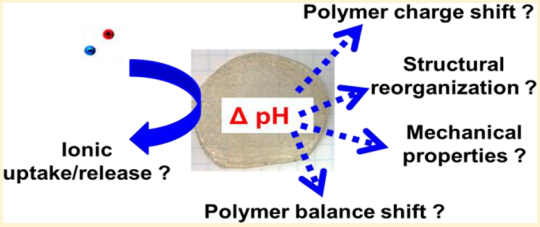

1. INTRODUCTION

Compact polyelectrolyte complexes (COPECs), also named saloplastics, were introduced in 2009, following the rediscovery that polyelectrolyte complexes can be plasticized in the presence of high salt concentrations and processed into bulk plastics by centrifugation.[1] Consequently, the recent years witnessed the synthesis of a variety of saloplastics and composites,[2] assembled from either synthetic[3] or natural[4−6] polyelectrolytes. The resulting COPECs exhibited high fracture strain (400%)[3] and self-healing properties.[7] These materials triggered applications mainly in the field of biomaterials by allowing the encapsulation of enzymes,[8] by providing matrices for tissue engineering,[4] or by mimicking the mechanical properties of cartilage.[9] In a recent case, a saloplastic based on the alginate/chitosan polyelectrolyte couple was found to repel both bacteria and cells.[6] To achieve such appealing properties, the chemical composition of COPECs, their microstructure, and their mechanical properties must be controlled. From the polymer science point of view, hydrated COPECs are promising materials because of their blending at the molecular level[10] that leads to interpenetrated networks. Physical interactions including chain entanglement and ion-pairing processes govern the cohesion of such saloplastics,[11] influencing their composition, microstructure, and mechanical properties.[3] It is thus critical to understand these mechanisms for the future development of functional materials. Although some hints can be obtained from the fields of polyelectrolyte complexes and multilayer films to predict the behavior of COPECs, their nature as "bulky" plastics composed of highly concentrated compacted polyelectrolyte complexes makes detailed comparison hazardous. As a matter of fact, the fundamental behavior of saloplastics with respect to post-

Received: March 21, 2018
Revised: May 21, 2018
Published: June 4, 2018

DOI: 10.1021/acs.macromol.8b00609
Macromolecules 2018, 51, 4424−4434

assembly pH changes remains totally unknown. This article aims at providing a multiscale understanding of the pH-responsiveness of saloplastics based on weak polyelectrolytes (Scheme 1). Poly(methacrylic acid) (PMAA) was used as a

Scheme 1. Structure of the Weak Polyelectrolytes Used and Their Possible Interactions after Pairing

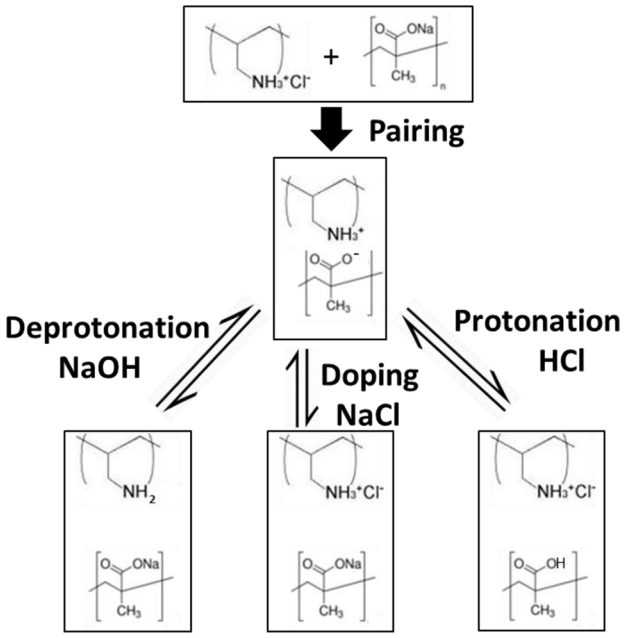

polyanion and poly(allylamine hydrochloride) (PAH) as a polycation, and the corresponding COPECs were prepared by centrifugation at pH 7 in 0.6 M NaCl. The effects of postassembly pH changes on PMAA/PAH COPECs were studied with respect to their ionization degree, ionic doping, microstructure, transition temperature, and mechanical properties.

2. RESULTS AND DISCUSSION

Compacted complexes of poly(methacrylic acid) (PMAA)/poly(allylamine hydrochloride) (PAH) were elaborated by mixing the two polymers in an equimolar concentration (with respect to their monomer units) at pH 7 and in 0.6 M NaCl. The obtained primary complexes were compacted by centrifugation at 3500*g* for 30 min, leading to the formation of PMAA/PAH saloplastics. Such a low centrifugal force, compared to the 188 000*g* force required for assembling poly(acrylic acid)/poly(allyamine hydrochloride) (PAA/PAH) saloplastics,[3] is related to the additional methyl group on the backbone of PMAA. This small structural change makes PMAA bulkier and slightly more hydrophobic than PAA. This allows PMAA to partly self-associate via hydrophobic interactions when PMAA/PAH complexes are formed in the presence of a high ionic force.[12] The resulting complexes are bigger, less ordered, and less dense than PAA/PAH complexes, allowing their processing into saloplastics by using a lower centrifugal force. These raw COPECs were processed into 1 mm thick disks by compression between two poly(methyl methacrylate) plates for 12 h. The corresponding COPEC disks were analyzed by using attenuated total reflection infrared spectroscopy (ATR-FTIR) (Figure S-1). The inclusion of both PMAA and PAH in the saloplastic was confirmed as denoted by ATR-FTIR absorption bands localized at 1545 cm^{-1} (COO^- asymmetric stretching), 1620 cm^{-1} (NH_3^+ asymmetric deformation), and 1020 cm^{-1} (primary amine C−N stretching).[13] XPS analysis on such COPECs revealed an atomic ratio O/N of 1.98 to be compared with an expected ratio of 2.00 for an equimolar concentration in PMAA and PAH monomers (Figure S-2). After drying PMAA/PAH COPECs under vacuum for 12 h, a semitransparent material was obtained (Figure 1a), owing to its

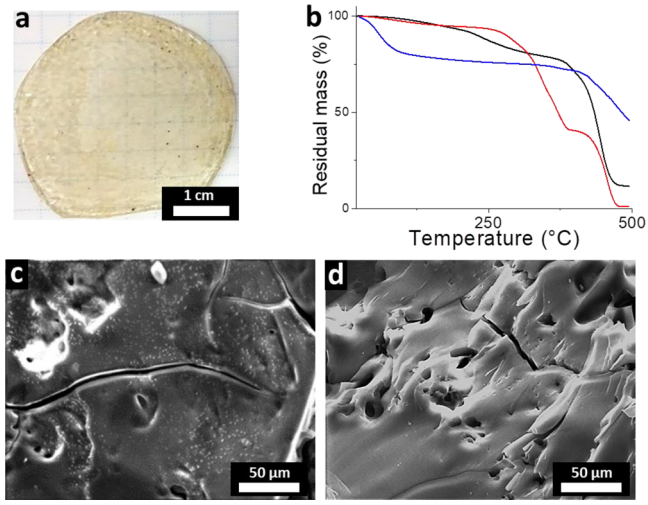

Figure 1. General characterization of PMAA/PAH-based COPECs. (a) Typical dry COPEC obtained after vacuum drying PMAA/PAH saloplastic disks assembled in 0.6 M NaCl at pH 7. (b) Thermogravimetric analysis of the corresponding dry COPECs (black line) and its components PAH (red line) and PMAA (blue line) from room temperature to 500 °C under argon at a rate of 10 °C/min. Typical SEM micrographs of (c) the surface and (d) the cross section of dry PMAA/PAH COPECs obtained at pH 7 in 0.6 M NaCl.

flat surface and limited porosity (Figure 1c,d). This result can be compared with previously reported extruded complexes of poly(styrenesulfonate) (PSS)/poly(diallyldimethylammonium chloride) (PDADMAC) that exhibited similar semitransparency.[14]

The thermal degradation of PMAA and PAH was analyzed by thermogravimetric analysis (TGA) both before and after their inclusion in COPECs. PAH exhibited three clear thermal regimes identified as the release of water bound molecules (5% mass loss from 40 to 150 °C), followed by the elimination of pendant NH_3^+ groups (54% mass loss from 150 to 380 °C) and ultimately the degradation of the polymeric backbone leaving to a nearly total combustion of PAH (Figure 1b).[15,16] In contrast, PMAA did not fully degrade at 500 °C and retained 45% of its mass. It exhibited three thermal regimes identified as the release of water bound molecules (22% mass loss from 40 to 150 °C), followed by a stable regime during which carboxylic functions underwent cyclization to form anhydrides groups (around 250 °C) that ultimately underwent decarboxylation (from 380 °C), leading to the formation of aromatic structures.[17] The dried COPEC demonstrated a remarkable stability up to 370 °C, only losing 22% of its mass. Similar results were reported for COPECs based on PSS/PDADMAC, suggesting that such materials are suitable for performing extrusion processes, which typically require temperatures lower than 300 °C.[2,14] Interestingly, PMAA/PAH COPECs outperformed the thermal stability of PAH up to 370 °C. Such stabilization of the polymer blend was previously reported for PAA/PAH multilayer films

DOI: 10.1021/acs.macromol.8b00609
Macromolecules 2018, 51, 4424−4434

and attributed to the formation of interchain amide bonds at 220 °C that limits the elimination of pendant NH_3^+ groups from PAH.[15,18] In contrast, when COPECs were first treated with formaldehyde prior to performing TGA, the thermal stability of COPECs was significantly reduced, retaining only 40% of their initial mass at 370 °C versus 78% for nontreated COPECs (Figure S-3). Upon exposure to formaldehyde, the ATR-FTIR spectrum of COPECs revealed a significant decrease of the NH_3^+ symmetric deformation band localized at 1510 cm^{-1} and the appearance of a secondary amine C−N stretching band at 1340 cm^{-1} (Figure S-3).[19,20] These results suggest that primary amines from PAH were converted to secondary amine groups when exposed to formaldehyde, thus limiting their ability to form amide bonds and to stabilize the COPECs.[21]

2.1. Ionization State of Polymers in Response to pH Stimuli. COPECs are formed by mixing polycations and polyanions whose charge is compensated either by polyelectrolyte−polyelectrolyte interaction (intrinsic charge compensation mechanism) or by interacting with counterions (extrinsic compensation mechanism).[22,23] In the field of polyelectrolyte assemblies, a range of experimental parameters was found to influence the charge compensation process, including the relative polymer molecular weights,[24] the polymer charge density,[25,26] the ionic strength of the environment,[27,28] and the nature of the counterions.[29] In the field of COPECs, changing the pH during the synthesis of saloplastics based on weak polyelectrolytes resulted in tuning their composition. Typically, the polyelectrolyte with the lowest charge density became more concentrated in the final material.[3] In contrast, little is known when the pH change occurs after the COPEC synthesis, i.e., after both polyelectrolyte pairing and charge compensation processes. Here, COPECs based on weak polyelectrolytes PMAA and PAH were elaborated at pH 7 in 0.6 M NaCl and then incubated for 12 h at pH 3, 4.5, and 9 in 0.6 M NaCl. When COPECs were incubated at pH lower than 3 and higher than 9, they dissolved in less than 12 h. The ionization rate of PMAA at different pH was calculated from the ATR-FTIR spectra of COPEC.[15,30] Deconvolution of the ATR-FTIR composite peaks at 1500−1570 and 1600−1700 cm^{-1} revealed the contributions of COO^- (1545 cm^{-1} asymmetric stretching), COOH, and associated COOH (1698 and 1660 cm^{-1}, stretching) from PMAA as well as the asymmetric (1620 cm^{-1}) and symmetric (1510 cm^{-1}) deformations of NH_3^+ from PAH (Figure S-4).[31] The ionization degree of PMAA in the COPEC, D^{pH}_{PMAA}, was calculated as a function of the pH by assuming that COOH and COO^- have similar extinction coefficients, as follows:

$$D^{pH}_{PMAA}\ (\%) = \frac{A^{pH}_{COO^-}}{A^{pH}_{COO^-} + A^{pH}_{COOH}(\text{free}) + A^{pH}_{COOH}(\text{assoc.})} \times 100$$

For calculating the ionization degree of PAH, the areas of ATR-FTIR peaks localized at 2920 cm^{-1} (CH_2 stretching) and 3000 cm^{-1} (NH_3^+ stretching) were used (Figure S-5). These peaks did not overlap; thus, direct calculation from their respective areas was possible. The ionization degree of PAH in the COPEC and as a function of the pH, D^{pH}_{PAH}, was calculated as follows:

$$D^{pH}_{PAH}\ (\%) = \frac{A^{pH}_{NH_3^+}/A^{pH}_{CH_2}}{A^{pH\ 3}_{NH_3^+}/A^{pH\ 3}_{CH_2}} \times 100$$

The ionization degree D^{pH}_{PMAA} in the COPEC increased rapidly from 14% at pH 3, where PMAA is poorly water soluble, to 78% at pH 9 (Figure 2). Although following the same trend,

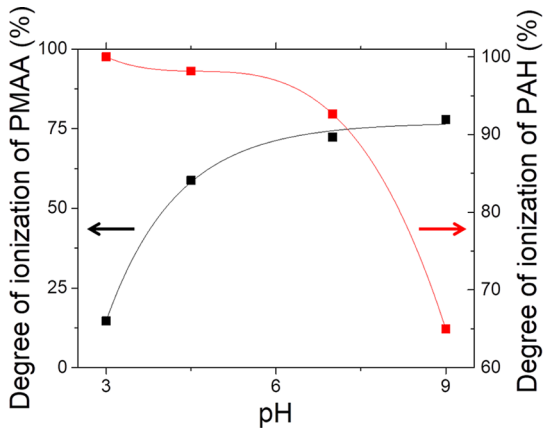

Figure 2. Ionization state of PMAA (D^{pH}_{PMAA}) and PAH (D^{pH}_{PAH}) in COPECs as a function of the pH. The degrees of ionization of PAH (red line) and PMAA (black line) were calculated according to Rubner et al.[30] from IR absorption transitions corresponding to $N-H_3^+$ stretching (3000 cm^{-1}), $C-H_2$ stretching (2920 cm^{-1}), COO^- asymmetric stretching (1545 cm^{-1}), and COOH stretching (1660−1700 cm^{-1}).

these results are smaller than the ionization degree previously found for PAA in PAA/PAH multilayer films, probably because the pK_a of methacrylic acid monomers is higher (4.7) than the pK_a of acrylic acid monomers (4.25).[32] In contrast, the ionization degree D^{pH}_{PAH} changed in a much narrower window, decreasing from 98% at pH 4.5 to 65% at pH 9. (Figure 2) These results are similar to the D^{pH}_{PAH} found in PAA/PAH multilayer films.[30]

2.2. Polyelectrolyte and Charge Balances in COPECs in Response to pH Stimuli. Changing the pH of the solution in contact with the COPEC induced considerable change in the charge density of both PMAA and PAH. The perturbation of the charge balance within the COPEC upon pH changes can be compensated either by (i) releasing polyelectrolyte chains to restore the initial charge balance, which is likely to modify the COPEC's composition, and (ii) using intrinsic and extrinsic charge compensation mechanisms to accommodate the charge imbalance, which is likely to modify the COPEC's morphology and its concentration in counterions. Both hypotheses were investigated by using ATR-FTIR spectroscopy. The monomer balance $P^{pH}_{PMAA/PAH}$ in PMAA/PAH COPECs was first calculated as a function of the pH. The FTIR peaks localized at 1010 cm^{-1} (C−N stretch, from PAH) and 1340 cm^{-1} ($C-H_3$ bending, mainly from PMAA) were used, and the $P^{pH}_{PMAA/PAH}$ was fixed to 1 at pH 7, in accordance with XPS data (Figure 3, Figures S-2 and S-6).

$$P^{pH}_{PMAA/PAH} = \frac{A^{pH}_{CH_3}/A^{pH}_{NH}}{A^{pH\ 7}_{CH_3}/A^{pH\ 7}_{NH}}$$

Deviations from equimolarity occurred at both pH 3 and 9, signaling an excess of PMAA at pH 3 (ratio of 1.28) and an excess of PAH at pH 9 (ratio of 0.91). This trend has also been reported by Reisch et al., where the assembly pH of PAA/PAH COPECs changed during their elaboration.[3] Yet, in our study, the amplitude of the change of $P^{pH}_{PMAA/PAH}$ was attenuated.

DOI: 10.1021/acs.macromol.8b00609
Macromolecules 2018, 51, 4424−4434

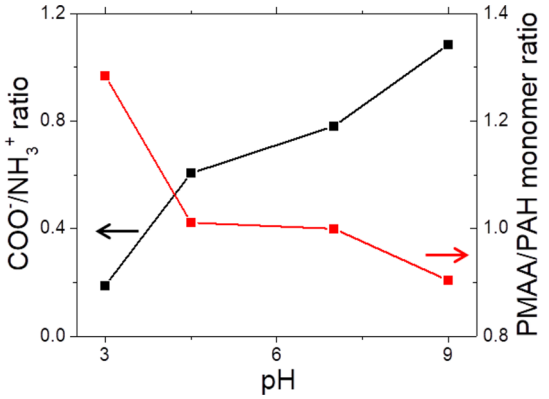

Figure 3. Evolution of the monomer balance and of their charge ratio within COPEC. Evolution of the monomer balance (red line) and of the ratio of charged units (black line) in PMAA/PAH COPECs as a function of the incubation pH and calculated from ATR-FTIR data (red line). COPECs were first prepared at pH 7 in 0.6 M NaCl followed by incubation for 12 h in a 0.6 M NaCl solution at the considered pH before performing ATR-FTIR.

Changing the pH after the polyelectrolyte pairing has thus a more limited, or slower, effect on COPECs compared with changing the assembly pH. These results illustrate the dynamic composition of saloplastics, that is, when the charge density of PMAA (PAH) decreased, polyelectrolyte chains of PAH (PMAA) were released from the COPEC. Such a dynamic behavior opens application perspectives for COPECs in the field of self-healing materials.[33] This phenomenon could allow reducing the pH-induced charge imbalance in the saloplastics, which confirms our first hypothesis (i). To investigate if the sole release of polyelectrolyte chains succeeded in counteracting the pH-induced charge imbalance in COPECs, the evolution of the COO^-/NH_3^+ ratio in the saloplastics was calculated as a function of the pH (Figure 3):

$$R^{pH}_{COO^-/NH_3^+} = \frac{D^{pH}_{PMAA}}{D^{pH}_{PAH}} \times P^{pH}_{PMAA/PAH}$$

If the release of polyelectrolyte chains was strong enough to preserve the charge balance in PMAA/PAH saloplastics, $R^{pH}_{COO^-/NH_3^+}$ had to remain independent from the incubation pH. On the contrary, this ratio was found to evolve dramatically with the pH, reaching 0.19 at pH 3 and 1.05 at pH 9 (Figure 3). This result demonstrates that a significant part of the pH-induced charge imbalance in COPECs remained after the release of polyelectrolyte chains. The emergence of such "free" charged groups within the saloplastics may thus be compensated by intrinsic and extrinsic charge compensation mechanisms, as hypothesized in (ii). The relationship between the evolution of the COO^-/NH_3^+ ratio and the molality of Na^+ counterions in COPECs was thus investigated.

2.3. Molality of Na^+ Counterions in Response to pH Stimuli. The molality of Na^+ ions in dry COPECs was measured by inductively coupled plasma mass spectroscopy (ICP) in saloplastics incubated in 0.6 M NaCl solutions at pH 3, 4.5, 7, and 9. The Na^+ molality in dry COPECs was corrected by taking into account of their water content (W^{pH}), obtained from TGA data (Figure S-7). The Na^+ molality ($b^{pH}_{Na^+}$(wet)) in wet COPECs was thus calculated as a function of the pH as follows (Figure 4):

$$b^{pH}_{Na^+}(\text{wet}) = b^{pH}_{Na^+}(\text{dry})/(1 + W^{pH})$$

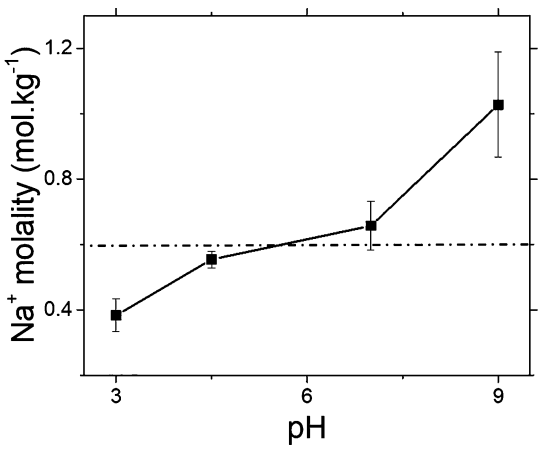

Figure 4. Na^+ molality in wet COPECs as a function of the incubation pH. Evolution of the molality of Na^+ ions in wet COPECs as a function of the incubation pH and calculated from ICP and TGA data (black line). The dotted line represents the initial Na^+ molality (0.6 mol kg^{-1}) in the solution of incubation.

Na^+ ions are likely to exist in COPEC either as a NaCl pair within the pores of the material or as a counterion of carboxylate functions born by PMAA. The evolution of both $b^{pH}_{Na^+}$(wet) showed a striking similarity with the evolution of $R^{pH}_{COO^-/NH_3^+}$ as a function of the incubating pH (Figures 3 and 4). This result demonstrates that Na^+ ions in COPECs predominantly exist as counterions for COO^- groups, confirming the role played by the extrinsic charge compensation mechanism upon pH-induced charge imbalance in COPECs. Controlling the availability of carboxylate groups within the saloplastic, by deprotonating either COOH from PMAA or NH_3^+ from PAH, provides thus a driving force governing the uptake of Na^+. Such stimulus-responsive uptake abilities make COPECs promising candidates for the reversible immobilization of drugs and enzymes.[8] The increase of $b^{pH}_{Na^+}$(wet) with the incubation pH is likely to influence the doping of PMAA chains as well as their ability to establish physical reticulation points with PAH. This phenomenon was studied by TGA, ICP, and differential scanning calorimetry (DSC).

2.4. Physical Reticulation Points within PMAA/PAH COPECs upon pH Stimuli. The partial dissolution of PAH (PMAA) chains at pH 3 (pH 9) indicates that the mobility of polymer chains within PMAA/PAH saloplastics changes with the pH (Figure 3). The density of ionic reticulation points between PMAA and PAH in saloplastics influences the polymer chains' mobility and ultimately the cohesion of COPECs. Upon pH changes, the cross-link density is likely to be governed by: (i) The relative proportion of polyelectrolytes and their ionization degree: more reticulation points are potentially available when PMAA is deprotonated and PAH protonated. (ii) The doping of polyelectrolytes with counterions: the extrinsic charge compensation mechanism refrains the formation of intrinsic polyelectrolyte−polyelectrolyte pairs. Within the pH window considered in this work, the molality of COO^- groups in COPECs is always inferior or equal to the molality of NH_3^+ groups (Figure 3). The density of potential reticulation points between PMAA and PAH is thus governed

DOI: 10.1021/acs.macromol.8b00609
Macromolecules 2018, 51, 4424−4434

by the molality of undoped COO^- groups in wet COPECs (Figure 5), calculated as

$$b^{pH}_{COO^-}(\text{available}) = b^{pH}_{COO^-}(\text{wet}) \times (1 - y^{pH}_{COO^-})$$

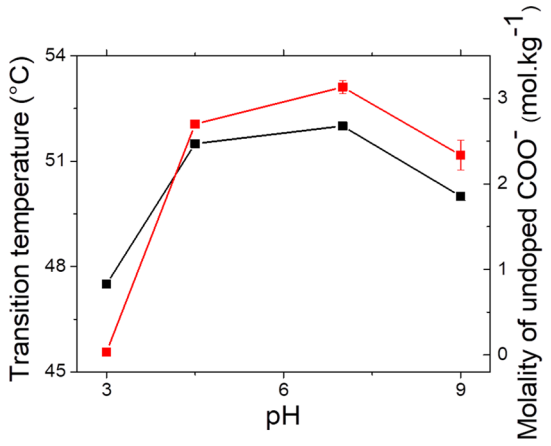

Figure 5. Transition temperature and molality of carboxylate groups available for reticulation. Evolution of the molality of undoped COO^- groups $b^{pH}_{COO^-}$(available) in wet COPECs (red line) as a function of the incubation pH. Evolution of the transition temperature of the saloplastics obtained from DSC data as a function of the pH (black line). COPECs were first prepared at pH 7 in 0.6 M NaCl followed by incubation for 12 h in a 0.6 M NaCl solution at the considered pH before performing DSC measurements.

with $b^{pH}_{COO^-}$(wet) the molality of carboxylate groups in wet COPECs and $y^{pH}_{COO^-}$ the doping rate of carboxylate groups with Na^+. A detailed description of the calculations is available in the Supporting Information and Figure S-8.

The molality of COO^- groups available for cross-linking with PAH in wet saloplastics evolved dramatically upon pH changes, reaching its maximum at pH 7. Almost all the carboxylic functions from PMAA were either protonated or doped with Na^+ ions at pH 3, when a strong excess of PMAA was measured in COPECs (Figures 3 and 5). At pH 3, PMAA in the saloplastic became both weakly charged and poorly soluble, while most of its remaining COO^- groups were extrinsically compensated with Na^+ (Figure S-8). The cross-link density with fully charged PAH chains was thus minimum, allowing PAH to dissolve out of the COPEC. At pH 9, too, the decrease in the molality of COO^- groups available for cross-linking the COPEC coincided with an imbalanced composition. In that case, the diminution of $b^{pH}_{COO^-}$(available) at pH 9 was rather attributed to the large uptake of Na^+ counterions, that doped around 50% of carboxylate groups (Figure S-8), allowing PMAA chains to dissolve out of the saloplastic. To confirm that the polymer chain mobility in PMAA/PAH COPECs undergoes pH-induced changes, DSC investigations were performed to measure the transition temperature (T_{tr}) of COPECs (Figure 5). The transition temperatures of both PAA/PAH and PSS/PDADMAC multilayer films were previously found to be sensitive to the assembly pH and the ionic force, respectively.[34,35] Here, the T_{tr} of dry PMAA/PAH COPECs was measured from the DSC data (Figure 5 and Figure S-9). T_{tr} remained stable around 51−52 °C from pH 4.5 to 7 but decreased at pH 3 and 9, reaching 47.5 and 50 °C, respectively, indicating that polymer chains are more mobile at pH extrema. These results were in accordance with the partial dissolution of COPECs at pH extrema calculated from the ATR-FTIR data (Figure 3). This trend was very similar to the molality evolution of undoped COO^- groups (Figures 5), confirming that the cross-link density within COPECs governs their polyelectrolyte chain mobility. Thus, changing the incubation pH of PMAA/PAH saloplastics gives access to tuning of the cross-link density within COPECs, either by protonation or by ionic doping of COO^- groups. The density of cross-link points in polyelectrolyte complexes and multilayers has also been shown to govern the water content of the assemblies. For instance, when PAA/PAH complexes were incubated at increasing pH, their water content decreased in commensuration with the deprotonation rate of PAA.[36] Here the water content of PMAA/PAH COPECs evolved by following the opposite trend as compared to $b^{pH}_{COO^-}$(available), reaching its maximum (65%) at pH 3 and its minimum (43%) at pH 9 (Figure S-7). The increase of the cross-link density between PMAA and PAH from pH 3 to pH 4.5−7 resulted in the release of the water molecules associated with ammonium groups from PAH, in agreement with the literature.[36]

Microstructural Properties. The influence of postassembly pH changes on the structure of PMAA/PAH COPECs was investigated by scanning electron microscopy (SEM). The morphological evolution of the cross-sectional view of saloplastics allowed estimating the pore density of such COPECs (Figure 6).

A dramatic change in the porosity upon pH changes was found, as testified by the pore coverage calculated from SEM data (Figure 6). If COPECs incubated at pH 7 and 9 exhibited

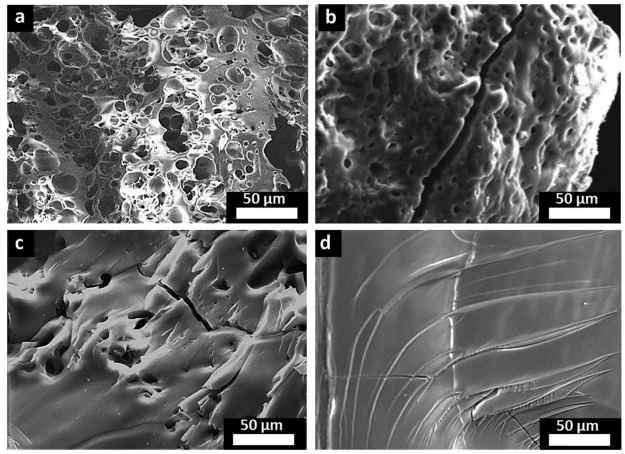

e pH	Average pore area (µm²)	Average pore density per 100 µm²
3	43.7 (6.3)	0.41(0.04)
4.5	36.4 (3.8)	0.36 (0.03)
7	51.2 (8.3)	0.11 (0.03)
9	1.05 (0.4)	0.12 (0.11)

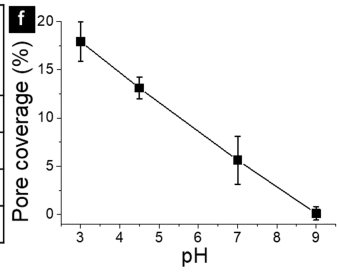

Figure 6. Microstructural properties of PMAA/PAH COPECs. Typical SEM micrographs of the cross-sectional view of COPECs after incubation for 12 h in a 0.6 M NaCl solution at pH 3 (a), 4.5 (b), 7 (c), and 9 (d). (e) Pore average areas and densities of the corresponding COPECs, obtained by software analysis of the micrographs. (f) Evolution of the average pore coverage of each micrograph as a function of the pH.

DOI: 10.1021/acs.macromol.8b00609
Macromolecules 2018, 51, 4424−4434

a cross section with little-to-no porosity, several pores emerged at lower pH, finally representing up to 18% of the micrograph's area (Figure 6f). Achieving a fine control of the COPEC's porosity is of importance for future applications in the field of purification membranes. For instance, the superior pervaporation performances of membranes based on dextran sulfate/chitosan sulfated saloplastics were recently attributed to their compact yet hydrated nature.[37,38] The formation of pores within polyelectrolyte materials can arise from several factors: an increase of the local osmotic pressure in the presence of a higher ionic strength,[28] a decrease in the material's cross-link density, or a mismatch between the number of positive and negative charges born by the polyelectrolyte chains.[39,40] In this work, the doping rate of COO^- groups with Na^+ ions (Figure S-8) did not correlate with the emergence of pores within the PMAA/PAH saloplastic, indicating that osmotic pressure was not a prominent factor. In contrast, both a lower density of potential reticulation points (Figure 5) and a mismatch in the polyelectrolyte charges (Figure 3) coincided with the emergence of pores at acidic pH within COPECs. The mismatch in the $R^{pH}_{COO^-/NH_3^+}$ ratio promotes indeed the formation of loopy polymer conformations within COPECs, while the smaller number of reticulation points increases the polymer chain mobility. We propose that the combination of these two factors is promoting the emergence of pores via a configuration with swollen loops of PAH and collapsed PMAA coils (Scheme 2).[35]

Scheme 2. Schematic Representation of the Proposed Mechanism Leading to the Formation of Pores in COPECs at Acidic pH

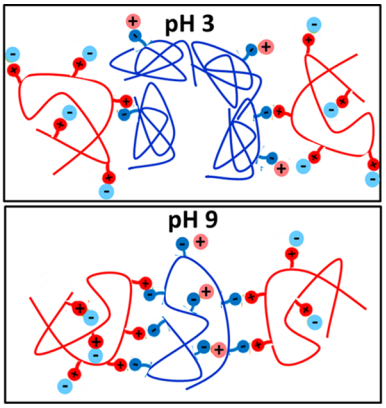

Charge Compensation Mechanism. The fact that the charge balance within the COPEC undergoes significant displacements upon pH changes means that new charges are available inside the saloplastic and need to be compensated either intrinsically or extrinsically. The starting pH of our experiments, that is pH 7, corresponds to the point where the charge densities on both polymers are close to their maximum. Increasing (decreasing) the pH results thus in the removal of charges on PAH (PMAA) chains. At pH extrema, the evolution of the transition temperature T_{tr}, the $P^{pH}_{PMAA/PAH}$ ratio, and the molality of undoped COO^- groups $b^{pH}_{COO^-}$(available) all indicated an increase of the polymer chain mobility (Figures 3 and 5). At these pH values, the doping rate of COO^- groups with Na^+ ions increased, suggesting that the extrinsic charge compensation mechanism was predominant in COPECs at pH 3 and 9 (Figure S-8). However, several compensation mechanisms are expected, if the charge removed on polymer chains was previously compensated intrinsically (I modes) or extrinsically (E modes) within the COPEC. With that respect, the charge compensation modes E_1 and I_2 (E_2 and I_1) tend to preserve (change) the ionic doping rate of COO^-, the density of PMAA/PAH cross-links, and the transition temperature T_{tr} of the COPECs (Scheme 3 and Table 1). Additional

Scheme 3. Schematic Representation of the Possible Charge Compensation Mechanisms, Described in a Table, as a Function of the Type of Electrostatic Pair Initially Disturbed by the pH Change[a]

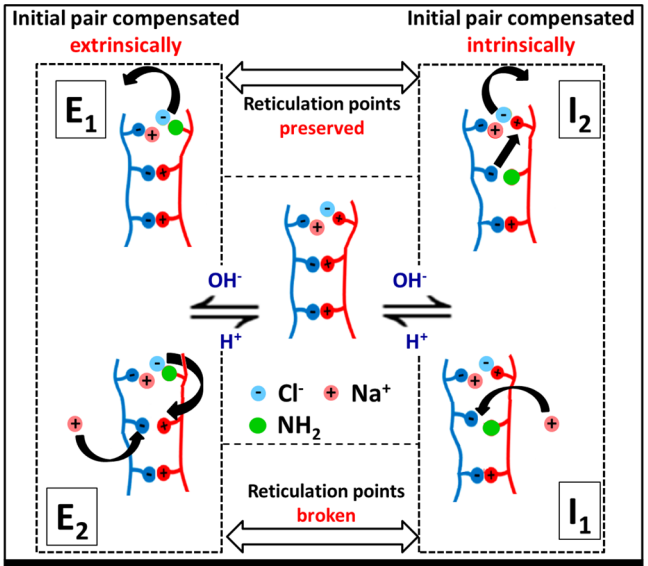

Initial pair	Compensation step 1	Compensation step 2	Name
Intrinsic pair	Ionic uptake	-	I_1
	Crosslink restored	Ionic expulsion	I_2
Extrinsic pair	Ionic expulsion	-	E_1
	Crosslink broken	Ionic uptake	E_2

[a]For sake of clarity, only the case of an increase of the pH is represented.

propagation of "sliding modes" is likely to affect the lubrication of polymer chains and thus T_{tr} (Scheme S-1), yet their termination ultimately results in either I_1 or I_2 modes.

Table 1. Possible Outcomes Induced by Specific Charge Compensation Mechanisms upon a Postassembly pH Change in COPECs

Compensation mode	Crosslink density	Na^+ doping of COO^-	T_{tr}
I_2, E_1	=	=	=
I_1, E_2	↘	↗	↘
Results (pH 4.5 to 7)	=/↗	=	=
Results (pH 3 and 9)	↘	↗	↘

DOI: 10.1021/acs.macromol.8b00609
Macromolecules 2018, 51, 4424−4434

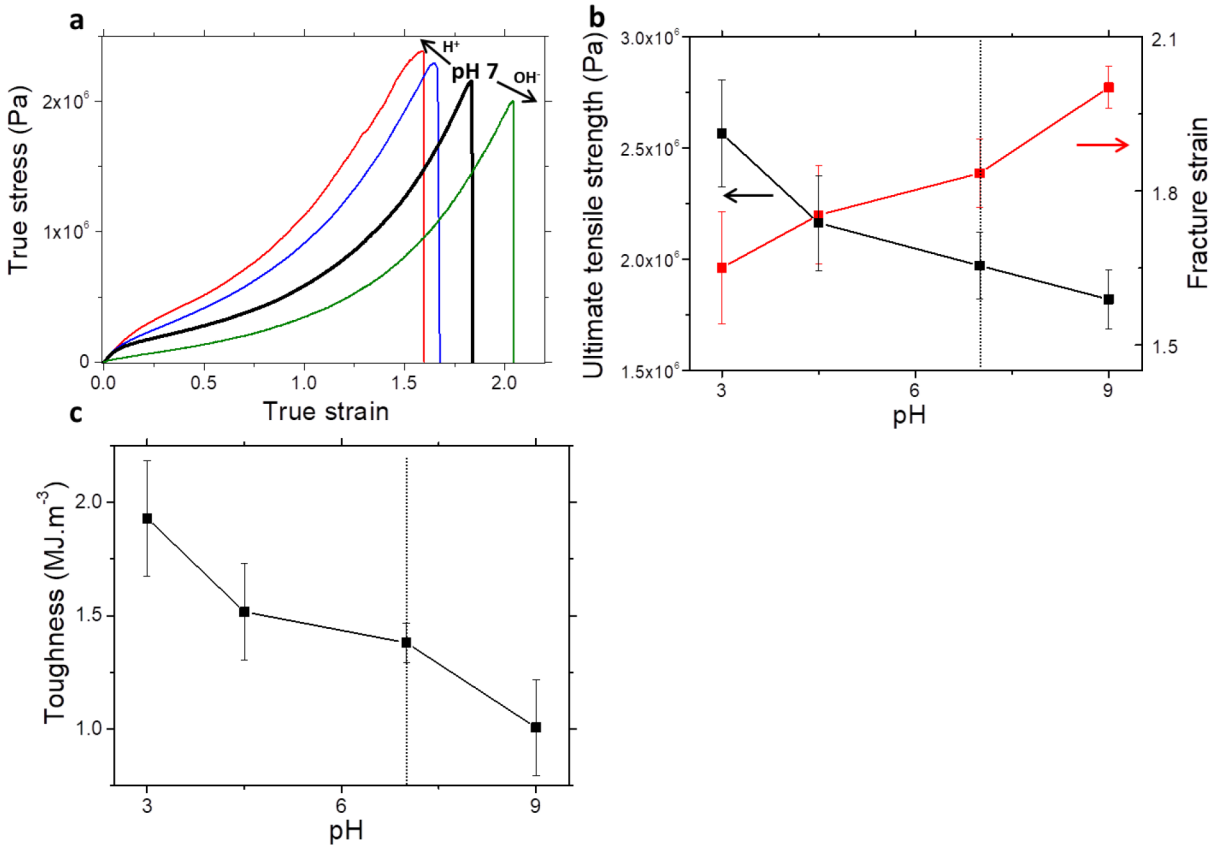

Figure 7. Mechanical properties of PMAA/PAH based COPECs. (a) Strain to break tests of wet COPEC ribbons immersed for 12 h in a 0.6 M NaCl solution at pH 3 (red line), 4.5 (blue line), 7 (black line), and 9 (green line). Corresponding evolution of the fracture strain and ultimate tensile strength (b) as a function of the incubation pH. (c) Toughness of the COPEC ribbons integrated from the strain to break curve as a function of the incubation pH. The initial pH at the start of the experiments is signaled by a dotted line.

The charge compensation modes I_2 and E_1 are associated with a mechanism that preserves the number of reticulation points between polymers, either because the charge loss was initially compensated extrinsically or because the broken intrinsic bond was restored (Scheme 3). In that case, the only effect of the disappearance of a charge on PAH or PMAA chains is the release of the corresponding counterion, keeping the doping rate of COO^- constant (Table 1). In contrast, I_1 and E_2 are associated with the decrease of the number of PMAA/PAH bonds combined with an increase of the doping rate of carboxylate groups. Although all these mechanisms are likely to occur simultaneously, a comparison with experimentally accessible data provides insights about the preferential charge compensation modes when the pH is changed (Table 1).

With that respect, two different charge compensation regimes emerged when PMAA/PAH COPECs were submitted to postassembly pH changes: from pH 4.5 to 7, both the doping rate of COO^- groups and the transition temperature of the saloplastics remained stable (Figure 5 and Figure S-8), indicating that the charge compensation modes I_2 and E_1 were prominent. This regime corresponds thus to a pH window where the charge density on PMAA and PAH is high enough to allow preserving the reticulation points between the polymers. The second regime emerged at pH extrema, where the doping rate of COO^- groups increased and the density of PMAA/PAH cross-links decreased, as testified by the evolution of T_{tr} and $P^{pH}_{PMAA/PAH}$. This behavior corresponds to the charge compensation modes I_1 and E_2 (Table 1).

2.7. Mechanical Properties. To evaluate how a change of pH can influence the macroscopic properties of PMAA/PAH COPECs, the mechanical properties of such saloplastics were investigated. Strain-to-break tests were performed on wet saloplastic ribbons cut into dog bone shapes and incubated at pH 3, 4.5, 7, and 9 in a 0.6 M NaCl solution for 12 h (Figure 7).

The mechanical properties of polymeric materials result from the interplay between their composition, cross-link density, water and salt content, and polymer chain conformation.[41,42] For instance, both water molecules and counterions are known to act as plasticizers in polyelectrolyte assemblies.[23,41,43] Here, changing the pH of PMAA/PAH saloplastics resulted in changing most of these parameters, sometimes following opposite trends. PMAA/PAH COPECs showed a ductile behavior, reaching elongation rates from 420% at pH 3 to 640% at pH 9, to be compared with 500% for PAA/PAH COPECs at pH 6–7.[7] Accordingly, the mechanical tests indicated that PMAA/PAH saloplastics tend to become softer and more ductile when the pH increased, achieving higher fracture strains but lower ultimate tensile strength (Figure 7b). At lower pH, the COPECs remained flexible but their stiffness and toughness increased (Figure 7c). In this study, pH changes were initiated from pH 7, which corresponds to the point where the cross-link density of PMAA/PAH COPECs is maximum (Figure 5). With that respect, changing the pH in COPECs resulted in decreasing the density of cross-links, either by protonation of PMAA at lower pHs or by ionic doping of COO^- groups at

DOI: 10.1021/acs.macromol.8b00609
Macromolecules 2018, 51, 4424–4434

higher pHs. However, these two phenomena lead to different effects on the properties of COPECs:

- At increasingly acidic pH, PMAA chains were largely protonated, leading to an imbalanced COO^-/NH_3^+ ratio (Figure 3) and a low cross-link density within COPECs (Figures 5). These factors favor a configuration with swollen loops of PAH and collapsed PMAA coils (Scheme 2), leading to a poor polyelectrolyte pairing, a high porosity and large water content of the saloplastics (Figure 6 and Figure S-7). This configuration is analogous to rigid aggregates or nanoparticles embedded in a softer matrix, a case that is known for reinforcing composite materials. For instance, doping PSS/PDADMAC saloplastics with iron oxide nanoparticles resulted in increasing their tensile strength and toughness.[2] Along the same line, the formation of PMAA collapsed coils at low pH lead to stiffer and tougher PMAA/PAH COPECs. The pH-responsive stiffening of saloplastics based on weak polyelectrolytes opens application perspectives in the field of self-defensive biomaterials that limit bacterial adhesion upon bacteria-induced acidification of the medium.[44]
- At pH 9, PMAA/PAH COPECs exhibited a balanced COO^-/NH_3^+ ratio (Figure 3) and a relatively high cross-link density (Figure 5). However, the molality of Na^+ ions in the COPEC significantly increased (Figure 4). These factors favor a configuration with both polyelectrolytes adopting a swollen loops conformation and a better pairing than at pH 3 (Scheme 2), as evidenced by the low porosity (Figure 6) and the low water content (Figure S-7). This configuration is analogous to polymeric interpenetrated networks blended at the molecular level, as expected for typical COPECs.[10] In such a case, the plasticizing effect of the ionic strength in saloplastics is a prominent factor.[7] Accordingly, the higher molality of Na^+ counterions within PMAA/PAH COPECs at high pH lead to softer and more ductile COPECs.

2.8. Transition Metal Ions Sorption Capacity. Strategies of water purification from metal cations by using polymers containing carboxylate groups have attracted a focused attention for years.[45] However, current approaches present several drawbacks, including the need to perform an additional purification step to separate the cation/carboxylate complexes formed from the clean water.[46] In addition, the apparent pK_a of materials containing high concentrations of carboxylic moieties is typically increased,[47,48] which shifts the optimum operating pH for water purification to values higher than pH 5.5−6.[49,50] Since transition metal cations like Ni^{2+} and Cu^{2+} tend to form hydroxide in these conditions, sorption materials efficient at acidic pH need to be developed. The COPEC approach offers a simple route for elaborating sorbent materials that can be processed into membranes, fibers, and powders,[49] ultimately allowing a direct separation from clean water.

The sorption performance of PMAA/PAH saloplastics toward a range of transition metal cations was evaluated at pH 3 and 4.5 (Figure 8). The sorption capacity of COPECs followed the Irving−Williams complex stability series, reaching its maximum for the sorption of Cu^{2+} ions and typically increasing with the incubating pH. At pH 4.5, the sorption of Cu^{2+} ions exceeded 170 mg g^{-1}, an excellent performance that usually requires an operating pH of 6.[49] The ionization behavior of PMAA (Figure 2), indicated that the pK_a of carboxylic moieties in the COPEC did not increase contrary to the apparent pK_a of other materials containing high concentrations of carboxylic groups, explaining the superior sorption abilities of PMAA/PAH saloplastics at acidic pH. This

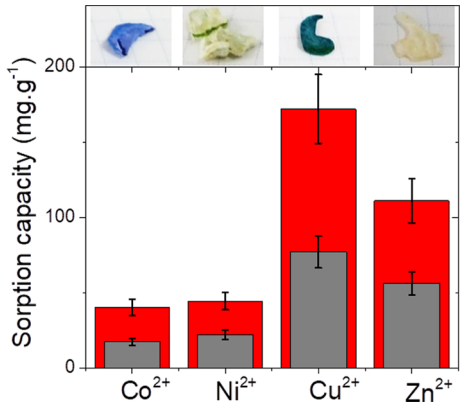

Figure 8. Sorption capacity and pictures of PMAA/PAH COPECs at pH 3 (gray bars) and 4.5 (red bars) toward transition metal cations after incubation for 12 h.

effect is ascribed to the ionic interaction between polycations and polyanions in the COPECs, favoring the deprotonation of weak polyelectrolytes.[51]

3. CONCLUSION

The response of PMAA/PAH COPECs to pH changes was studied with respect to their composition, charge balance, microstructure, water content, and concentration in Na^+ counterion and cross-link points. Since both PMAA and PAH are weak polyelectrolytes, it was possible to induce significant displacements in the charge balance within COPECs, initially assembled at pH 7. Facing such a misbalance, the response of PMAA/PAH COPECs was different depending on the pH window: (i) From pH 7 to 4.5, the charge compensation mechanism in the COPECs allowed preserving most of the PMAA/PAH reticulations points, allowing the stabilization of the polymer balance, doping rate of carboxylate groups, and transition temperature of the COPEC. (ii) At pH 3 and pH 9, the charge compensation mechanism lead to the breakage of PMAA/PAH bonds and an increase of the doping rate of carboxylate groups. This resulted in the destabilization of the polymer balance and a decrease of the transition temperature of the saloplastics. The macroscopic properties of PMAA/PAH COPECs, initially assembled at pH 7, evolved in a contrasted manner depending on the pH change, which evidenced that several mechanisms were acting. The water content of the saloplastics was governed by the density of PMAA/PAH cross-link points. In contrast, both the mechanical properties and the porosity of COPECs at acidic pH were governed by the conformation of PMAA chains. Stiffer and more porous saloplastics were obtained when the charge ratio was imbalanced and PMAA poorly soluble. At high pH, the intake of counterions lead to ductile softer COPECs with a modest porosity. PMAA/PAH saloplastics also exhibited excellent water purification properties at acidic pH, exceeding 170 mg g^{-1} sorption capacity for Cu^{2+} ions at pH 4.5, due to the low pK_a value of carboxylic groups in the COPECs. This work illustrates how a single basic change of the environment of COPECs can induce dramatic changes in their properties at multiple scales, including their microstructure and mechanical features (Scheme 4). Considering the range of responses provided by COPECs to a simple pH stimulus, there is no doubt that saloplastics will trigger applications in the field of stimuli-responsive materials in the future.

DOI: 10.1021/acs.macromol.8b00609
Macromolecules 2018, 51, 4424−4434

Scheme 4. Schematic Representation of the Multilevel Responses of PMAA/PAH COPECs to a pH Variation

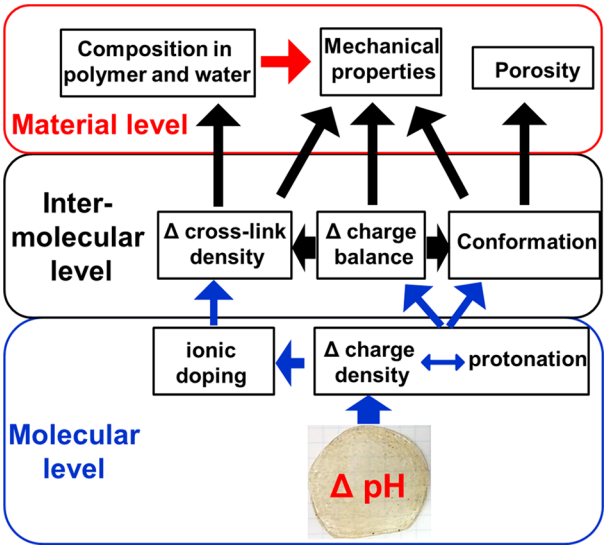

4. MATERIALS AND METHODS

Materials. Poly(methacrylic acid) (PMAA, CAS 25087-26-7 Polysciences Inc., M_w 100 000 g/mol) was neutralized in NaOH (0.2 M), dialyzed for 2 days against water, and lyophilized. Poly(allylamine hydrochloride) (PAH, CAS 71550-12-4, AlfaAesar, M_n 40 000 g/mol, M_w 104 000 g/mol) was used as received. Formaldehyde (CAS 50-00-0), $CuCl_2$ (CAS 7447-39-4), $CoCl_2$ (CAS 7646-79-9), $NiCl_2$ (CAS 7718-54-9), and $ZnCl_2$ (CAS 7646-85-7) were purchased from Sigma-Aldrich and used as received. NaCl (CAS 7647-14-5), NaOH (CAS 1310-73-2), and HCl (CAS 7647-01-0) were used to adjust the ionic strength and the pH of the polyelectrolyte solutions. Milli-Q water (Millipore), with a 18 MΩ resistance, was used to prepare all the solutions.

Synthesis of COPECs. Solutions PAH and PMAA were prepared at a concentration of 0.3 M with respect to their units, in 0.6 M NaCl at pH 7. Typically, 20 mL of each polyelectrolyte solution was poured simultaneously in a 200 mL beaker. The mixture was stirred with a magnetic stir bar at 400 rpm. The complexes formed were centrifuged at 3500*g* for 30 min. The obtained COPECs were compressed for 12 h in a fresh 0.6 M NaCl solution at pH 7 between two PMMA plates, allowing to form COPEC disks around 1 mm thick and 4 cm diameter.

Incubation. COPEC disks of 20 mm diameter and 1 mm thick were incubated in 500 mL of a 0.6 M NaCl at the desired pH for 12 h. The obtained COPECs were used fresh for ATR-FTIR, TGA, and strain to break measurements. For performing other measurements, the incubated COPECs were vacuum-dried overnight.

Reticulation. COPEC disks of 20 mm diameter and 1 mm thick were incubated in 100 mL of a 10% formaldehyde solution at pH 7 in the presence of 0.6 M NaCl.

Sorption of Transition Metal Cations. 1 g of COPEC was immersed for 12 h in 200 mL of a 0.2 M solution of the desired metal chloride salt at pH 3 or 4.5. The incubated COPECs were vacuum-dried overnight and analyzed by ICP.

Scanning Electron Microscopy (SEM). SEM was performed using a S-4800 apparatus (Hitachi, Japan) at accelerating voltages of 10 kV. The samples were first dried overnight under vacuum before observation. Calculation of the average pore areas and densities was performed from SEM data by using the ImageJ software.

Attenuated Total Reflection Infrared Spectroscopy (ATR-FTIR). ATR-FTIR on wet COPECs was performed by using a Thermo Scientific Nicolet 4700 apparatus (USA). The deconvolution and fit of ATR-FTIR peaks into Gaussian components was performed with the CasaXPS software.

Inductively Coupled Plasma Optical Emission Spectrometry (ICP). ICP was performed on a 20 mg sample of dry COPECs by using an ICPS8100CL model spectrometer.

Differential Scanning Calorimetry and Thermal Gravimetry Analysis (DSC and TGA). DSC and TGA were performed under argon on 15 mg of vacuum-dried or wet COPECs by using a SDT Q600 apparatus from TA Instruments (USA) with a heating rate of 10 °C/min. The second DSC scan was used for determining the transition temperatures of COPECs. The water content of COPECs was calculated by comparing the mass losses of wet and dry saloplastics at 180 °C:

$$W^{pH} = m^{pH}_{wet} - m^{pH}_{dry}$$

X-ray Photoelectron Spectroscopy (XPS). XPS was carried out on an ESCALAB Mark II (VG Company, U.K.)

Strain to Break Measurements. These measurements were performed at room temperature (22 °C) on wet COPECs cut into dog-bone-shaped ribbons of dimension 20 mm × 15 mm by using a Shimazu 100N apparatus (Shimazu, Japan).[52,53] A stretching speed of 10 mm/min was used. The true strain ϵ was calculated as

$$\epsilon = \ln\left(1 + \frac{\Delta l}{l_0}\right)$$

The true stress σ was calculated as

$$\sigma = \frac{F}{A}\left(1 + \frac{\Delta l}{l_0}\right)$$

with l and l_0 the length and the initial length of the ribbon in mm, F the force (N), and A the cross-sectional area of the ribbon (m^2). The toughness of the ribbons was calculated by integrating the area under the true stress/true strain (to failure) curve.[14]

Definition of the Main Calculated Parameters. D^{pH}_{PMAA} (%) and D^{pH}_{PAH} (%) are ionization rate of PMAA and PAH, calculated from ATR-FTIR data. $P^{pH}_{PMAA/PAH}$ is the ratio of polyelectrolytes In the COPECs, with respect to their monomer concentration, calculated from ATR-FTIR data. $R^{pH}_{COO^-/NH_3^+}$ is the charge balance within COPECs, calculated from ATR-FTIR data. $b^{pH}_{Na^+}$ is the molality (mol kg^{-1}) of Na^+ ions in either dry and wet COPECs, calculated from ICP and TGA data. $b^{pH}_{COO^-}$ is the molality (mol kg^{-1}) of COO^- groups in COPECs, calculated from ICP, TGA, and ATR-FTIR data. $y^{pH}_{COO^-}$ is the doping rate (%) of COO^- groups with Na^+ ions, calculated from ICP, TGA, and ATR-FTIR data (calculation details in the Supporting Information).

■ ASSOCIATED CONTENT

Supporting Information

The Supporting Information is available free of charge on the ACS Publications website at DOI: 10.1021/acs.macromol.8b00609.

ATR-FTIR spectra of COPECs (raw and deconvoluted spectra), XPS, TGA, DSC, and detailed calculations of $b^{pH}_{COO^-}$ (PDF)

■ AUTHOR INFORMATION

Corresponding Author

*E-mail Rydzekg@tcd.ie (G.R.).

ORCID

Gaulthier Rydzek: 0000-0002-2901-3441
Amir Pakdel: 0000-0001-5852-0808
Valeria Nicolosi: 0000-0002-7637-4813
Parvaneh Mokarian-Tabari: 0000-0002-5176-0478
Pierre Schaaf: 0000-0001-7423-5492
Fouzia Boulmedais: 0000-0002-4934-9276
Katsuhiko Ariga: 0000-0002-2445-2955

DOI: 10.1021/acs.macromol.8b00609
Macromolecules 2018, 51, 4424−4434

Funding

This work was supported by the International Center for Young Scientists (ICYS) and the Japanese Society for the Promotion of Science (JSPS).

Notes

The authors declare no competing financial interest.

■ ACKNOWLEDGMENTS

G.R. thanks the Material Analysis Station (NIMS) for ICP and XPS measurements as well as Dr. K. Kawakami and E. Satie for fruitful support.

■ REFERENCES

(1) Porcel, C. H.; Schlenoff, J. B. Compact Polyelectrolyte Complexes: "Saloplastic" Candidates for Biomaterials. *Biomacromolecules* **2009**, *10* (11), 2968−2975.
(2) Fu, J.; Wang, Q.; Schlenoff, J. B. Extruded Superparamagnetic Saloplastic Polyelectrolyte Nanocomposites. *ACS Appl. Mater. Interfaces* **2015**, *7* (1), 895−901.
(3) Reisch, A.; Tirado, P.; Roger, E.; Boulmedais, F.; Collin, D.; Voegel, J.-C.; Frisch, B.; Schaaf, P.; Schlenoff, J. B. Compact Saloplastic Poly(Acrylic Acid)/Poly(Allylamine) Complexes: Kinetic Control Over Composition, Microstructure, and Mechanical Properties. *Adv. Funct. Mater.* **2013**, *23* (6), 673−682.
(4) Costa, R. R.; Costa, A. M. S.; Caridade, S. G.; Mano, J. F. Compact Saloplastic Membranes of Natural Polysaccharides for Soft Tissue Engineering. *Chem. Mater.* **2015**, *27* (21), 7490−7502.
(5) Rodrigues, M. N.; Oliveira, M. B.; Costa, R. R.; Mano, J. F. Chitosan/Chondroitin Sulfate Membranes Produced by Polyelectrolyte Complexation for Cartilage Engineering. *Biomacromolecules* **2016**, *17* (6), 2178−2188.
(6) Phoeung, T.; Spanedda, M. V.; Roger, E.; Heurtault, B.; Fournel, S.; Reisch, A.; Mutschler, A.; Perrin-Schmitt, F.; Hemmerlé, J.; Collin, D.; et al. Alginate/Chitosan Compact Polyelectrolyte Complexes: A Cell and Bacterial Repellent Material. *Chem. Mater.* **2017**, *29* (24), 10418−10425.
(7) Reisch, A.; Roger, E.; Phoeung, T.; Antheaume, C.; Orthlieb, C.; Boulmedais, F.; Lavalle, P.; Schlenoff, J. B.; Frisch, B.; Schaaf, P. On the Benefits of Rubbing Salt in the Cut: Self-Healing of Saloplastic PAA/PAH Compact Polyelectrolyte Complexes. *Adv. Mater.* **2014**, *26* (16), 2547−2551.
(8) Tirado, P.; Reisch, A.; Roger, E.; Boulmedais, F.; Jierry, L.; Lavalle, P.; Voegel, J.-C.; Schaaf, P.; Schlenoff, J. B.; Frisch, B. Catalytic Saloplastics: Alkaline Phosphatase Immobilized and Stabilized in Compacted Polyelectrolyte Complexes. *Adv. Funct. Mater.* **2013**, *23* (38), 4785−4792.
(9) Hariri, H. H.; Schlenoff, J. B. Saloplastic Macroporous Polyelectrolyte Complexes: Cartilage Mimics. *Macromolecules* **2010**, *43* (20), 8656−8663.
(10) Oyama, H. T.; Frank, C. W. Structure of the Polyion Complex between Poly(Sodium P-Styrene Sulfonate) and Poly(Diallyl Dimethyl Ammonium Chloride). *J. Polym. Sci., Part B: Polym. Phys.* **1986**, *24* (8), 1813−1821.
(11) Shamoun, R. F.; Hariri, H. H.; Ghostine, R. A.; Schlenoff, J. B. Thermal Transformations in Extruded Saloplastic Polyelectrolyte Complexes. *Macromolecules* **2012**, *45* (24), 9759−9767.
(12) Gärdlund, L.; Wågberg, L.; Norgren, M. New Insights into the Structure of Polyelectrolyte Complexes. *J. Colloid Interface Sci.* **2007**, *312* (2), 237−246.
(13) Lin-Vien, D.; Colthup, N. B.; Fateley, W. G.; Grasselli, J. G. In *The Handbook of Infrared and Raman Characteristic Frequencies of Organic Molecules*; Academic Press: San Diego, CA, 1991; Chapter 10, pp 155−178.
(14) Shamoun, R. F.; Reisch, A.; Schlenoff, J. B. Extruded Saloplastic Polyelectrolyte Complexes. *Adv. Funct. Mater.* **2012**, *22* (9), 1923−1931.
(15) Shao, L.; Lutkenhaus, J. L. Thermochemical Properties of Free-Standing Electrostatic Layer-by-Layer Assemblies Containing Poly-(Allylamine Hydrochloride) and Poly(Acrylic Acid). *Soft Matter* **2010**, *6* (14), 3363−3369.
(16) Dragan, E. S.; Mihai, M.; Airinei, A. Thermochemically Induced Binding of Methyl Orange to Polycations Containing Primary Amine Groups. *J. Polym. Sci., Part A: Polym. Chem.* **2006**, *44* (20), 5898−5908.
(17) Grant, D. H.; Grassie, N. The Thermal Decomposition of Polymethacrylic Acid. *Polymer* **1960**, *1*, 125−134.
(18) Jang, W.-S.; Jensen, A. T.; Lutkenhaus, J. L. Confinement Effects on Cross-Linking within Electrostatic Layer-by-Layer Assemblies Containing Poly(Allylamine Hydrochloride) and Poly(Acrylic Acid). *Macromolecules* **2010**, *43* (22), 9473−9479.
(19) Brissette, C.; Sandorfy, C. Hydrogen Bonding in the Amine Hydrohalides: Ii. the Infrared Spectrum from 4000 to 2200 Cm−1. *Can. J. Chem.* **1960**, *38* (1), 34−44.
(20) Chenon, B.; Sandorfy, C. Hydrogen Bonding in the Amine Hydrohalides: I. General Aspects. *Can. J. Chem.* **1958**, *36* (8), 1181−1206.
(21) Ichinose, I.; Mizuki, S.; Ohno, S.; Shiraishi, H.; Kunitake, T. Preparation of Cross-Linked Ultrathin Films Based on Layer-by-Layer Assembly of Polymers. *Polym. J.* **1999**, *31*, 1065−1070.
(22) Fu, J.; Schlenoff, J. B. Driving Forces for Oppositely Charged Polyion Association in Aqueous Solutions: Enthalpic, Entropic, but Not Electrostatic. *J. Am. Chem. Soc.* **2016**, *138* (3), 980−990.
(23) Fares, H. M.; Schlenoff, J. B. Equilibrium Overcompensation in Polyelectrolyte Complexes. *Macromolecules* **2017**, *50* (10), 3968−3978.
(24) Sui, Z.; Salloum, D.; Schlenoff, J. B. Effect of Molecular Weight on the Construction of Polyelectrolyte Multilayers: Stripping versus Sticking. *Langmuir* **2003**, *19* (6), 2491−2495.
(25) Glinel, K.; Moussa, A.; Jonas, A. M.; Laschewsky, A. Influence of Polyelectrolyte Charge Density on the Formation of Multilayers of Strong Polyelectrolytes at Low Ionic Strength. *Langmuir* **2002**, *18* (4), 1408−1412.
(26) Steitz, R.; Jaeger, W.; Klitzing, R. v. Influence of Charge Density and Ionic Strength on the Multilayer Formation of Strong Polyelectrolytes. *Langmuir* **2001**, *17* (15), 4471−4474.
(27) Sukhorukov, G. B.; Schmitt, J.; Decher, G. Reversible Swelling of Polyanion/Polycation Multilayer Films in Solutions of Different Ionic Strength. *Berichte Bunsenges. Für Phys. Chem.* **1996**, *100* (6), 948−953.
(28) Mjahed, H.; Voegel, J.-C.; Senger, B.; Chassepot, A.; Rameau, A.; Ball, V.; Schaaf, P.; Boulmedais, F. Hole Formation Induced by Ionic Strength Increase in Exponentially Growing Multilayer Films. *Soft Matter* **2009**, *5* (11), 2269−2276.
(29) Fu, J.; Fares, H. M.; Schlenoff, J. B. Ion-Pairing Strength in Polyelectrolyte Complexes. *Macromolecules* **2017**, *50* (3), 1066−1074.
(30) Choi, J.; Rubner, M. F. Influence of the Degree of Ionization on Weak Polyelectrolyte Multilayer Assembly. *Macromolecules* **2005**, *38* (1), 116−124.
(31) Coates, J.; Coates, J. Interpretation of Infrared Spectra, A Practical Approach, Interpretation of Infrared Spectra, A Practical Approach. In *Encyclopedia of Analytical Chemistry*; John Wiley & Sons, Ltd.: 2006.
(32) Sonia, T. A.; Sharma, C. P. 6-Polymers in Oral Insulin Delivery. In *Oral Delivery of Insulin*; Woodhead Publishing Series in Biomedicine; Woodhead Publishing: 2014; pp 257−310.
(33) Schaaf, P.; Schlenoff, J. B. Saloplastics: Processing Compact Polyelectrolyte Complexes. *Adv. Mater.* **2015**, *27* (15), 2420−2432.
(34) Vidyasagar, A.; Sung, C.; Gamble, R.; Lutkenhaus, J. L. Thermal Transitions in Dry and Hydrated Layer-by-Layer Assemblies Exhibiting Linear and Exponential Growth. *ACS Nano* **2012**, *6* (7), 6174−6184.
(35) Vidyasagar, A.; Sung, C.; Losensky, K.; Lutkenhaus, J. L. PH-Dependent Thermal Transitions in Hydrated Layer-by-Layer Assemblies Containing Weak Polyelectrolytes. *Macromolecules* **2012**, *45* (22), 9169−9176.

DOI: 10.1021/acs.macromol.8b00609
Macromolecules 2018, 51, 4424−4434

(36) Zhang, Y.; Li, F.; Valenzuela, L. D.; Sammalkorpi, M.; Lutkenhaus, J. L. Effect of Water on the Thermal Transition Observed in Poly(Allylamine Hydrochloride)-Poly(Acrylic Acid) Complexes. *Macromolecules* **2016**, *49* (19), 7563−7570.
(37) Wang, X.-S.; Ji, Y.-L.; Zheng, P.-Y.; An, Q.-F.; Zhao, Q.; Lee, K.-R.; Qian, J.-W.; Gao, C.-J. Engineering Novel Polyelectrolyte Complex Membranes with Improved Mechanical Properties and Separation Performance. *J. Mater. Chem. A* **2015**, *3* (14), 7296−7303.
(38) Ji, Y.-L.; Gu, B.-X.; An, Q.-F.; Gao, C.-J. Recent Advances in the Fabrication of Membranes Containing "Ion Pairs" for Nanofiltration Processes. *Polymers* **2017**, *9* (12), 715.
(39) Elzbieciak, M.; Zapotoczny, S.; Nowak, P.; Krastev, R.; Nowakowska, M.; Warszynski, P. Influence of PH on the Structure of Multilayer Films Composed of Strong and Weak Polyelectrolytes. *Langmuir* **2009**, *25* (5), 3255−3259.
(40) Tjipto, E.; Quinn, J. F.; Caruso, F. Layer-by-layer Assembly of Weak-strong Copolymer Polyelectrolytes: A Route to Morphological Control of Thin Films. *J. Polym. Sci., Part A: Polym. Chem.* **2007**, *45* (18), 4341−4351.
(41) Zhang, R.; Zhang, Y.; Antila, H. S.; Lutkenhaus, J. L.; Sammalkorpi, M. Role of Salt and Water in the Plasticization of PDAC/PSS Polyelectrolyte Assemblies. *J. Phys. Chem. B* **2017**, *121* (1), 322−333.
(42) Ghostine, R. A.; Shamoun, R. F.; Schlenoff, J. B. Doping and Diffusion in an Extruded Saloplastic Polyelectrolyte Complex. *Macromolecules* **2013**, *46* (10), 4089−4094.
(43) Hariri, H. H.; Lehaf, A. M.; Schlenoff, J. B. Mechanical Properties of Osmotically Stressed Polyelectrolyte Complexes and Multilayers: Water as a Plasticizer. *Macromolecules* **2012**, *45* (23), 9364−9372.
(44) Saha, N.; Monge, C.; Dulong, V.; Picart, C.; Glinel, K. Influence of Polyelectrolyte Film Stiffness on Bacterial Growth. *Biomacromolecules* **2013**, *14* (2), 520−528.
(45) Dutta, K.; De, S. Smart Responsive Materials for Water Purification: An Overview. *J. Mater. Chem. A* **2017**, *5* (42), 22095−22112.
(46) Majumdar, D. Detoxification of Heavy Metal Ion-Contaminated Drinking Water by Green Technology-A Short Overview. *Curr. Green Chem.* **2017**, *4* (1), 38−44.
(47) Felberg, L. E.; Doshi, A.; Hura, G. L.; Sly, J.; Piunova, V. A.; Swope, W.; Rice, J.; Miller, R.; Head-Gordon, T. Structural Transition of Nanogel Star Polymers with PH by Controlling PEGMA Interactions with Acid or Base Copolymers. *Mol. Phys.* **2016**, *114* (21), 3221−3231.
(48) Schüwer, N.; Klok, H.-A. Tuning the PH Sensitivity of Poly(Methacrylic Acid) Brushes. *Langmuir* **2011**, *27* (8), 4789−4796.
(49) Lin, Y.; Hong, Y.; Song, Q.; Zhang, Z.; Gao, J.; Tao, T. Highly Efficient Removal of Copper Ions from Water Using Poly(Acrylic Acid)-Grafted Chitosan Adsorbent. *Colloid Polym. Sci.* **2017**, *295* (4), 627−635.
(50) Yan, H.; Dai, J.; Yang, Z.; Yang, H.; Cheng, R. Enhanced and Selective Adsorption of Copper(II) Ions on Surface Carboxymethylated Chitosan Hydrogel Beads. *Chem. Eng. J.* **2011**, *174* (2), 586−594.
(51) Skorb, E. V.; Möhwald, H.; Andreeva, D. V. How Can One Controllably Use of Natural ΔpH in Polyelectrolyte Multilayers? *Adv. Mater. Interfaces* **2017**, *4* (1), 1600282.
(52) Nicholson, J. *The Chemistry of Polymers*; Royal Society of Chemistry: 2017.
(53) Billmeyer, F. W. *Textbook of Polymer Science*; Wiley-Interscience: 1971.

DOI: 10.1021/acs.macromol.8b00609
Macromolecules 2018, 51, 4424−4434